INTERNATIONAL JOURNAL FOR NUMERICAL METHODS IN ENGINEERING
Int. J. Numer. Meth. Engng 2002; **53**:1415–1432 (DOI: 10.1002/nme.343)

A flux-limited numerical method for solving the MHD equations to simulate propulsive plasma flows

K. Sankaran[1,†], L. Martinelli[1], S. C. Jardin[2] and E. Y. Choueiri[1,*,‡]

[1] *Mechanical and Aerospace Engineering Department, Princeton University, Princeton, NJ 08544, U.S.A.*
[2] *Astrophysics Department, Princeton University, Princeton, NJ 08544, U.S.A.*

SUMMARY

For numerical simulations to be effective tools in plasma propulsion research, a high-order accurate solver that captures MHD shocks monotonically and works reliably for strong magnetic fields is needed. For this purpose, a characteristics-based scheme for the MHD equations, with flux limiters to improve spatial accuracy, has been developed. In this method, the symmetric form of the MHD equations, accounting for waves propagating in all directions, are solved. The required eigensystem of axisymmetric MHD equations, with appropriate normalization, is presented. This scheme was validated with unsteady (Riemann problem) and force-free equilibrium (Taylor state) test cases, as well as with measured current density patterns in a magnetoplasmadynamic thruster. Copyright © 2001 John Wiley & Sons, Ltd.

KEY WORDS: local extremum diminishing schemes; characteristics splitting; MHD solvers; plasma propulsion

1. INTRODUCTION

1.1. Motivation

Electromagnetic plasma propulsion systems offer significantly higher exhaust velocities than chemical propulsion systems, and process more power and produce higher thrust densities than space-charge limited electric propulsion systems. The fundamental acceleration process involves converting electrical energy into kinetic energy of the propellant, by the application of electromagnetic body forces. However, this simple explanation belies the complexity of the electromagnetic acceleration process, which embodies interlocking aspects of compressible gasdynamics, ionized gas physics, electromagnetic field theory, particle electrodynamics (as explained in Reference [1]) and plasma–surface interactions (as explained in Reference [2]).

*Correspondence to: Edgar Choueiri, Electric Propulsion and Plasma Dynamics Laboratory, Mechanical and Aerospace Engineering Department, Princeton University, Princeton, NJ 08544, U.S.A.
†E-mail: kamesh@princeton.edu
‡E-mail: choueiri@princeton.edu

Contract/grant sponsor: NASA-JPL's Advanced Propulsion Group

Received 3 November 2000
Revised 11 March 2001

The resulting theoretical complexity makes realistic description of the flow analytically intractable.

The electrical power deposited into the plasma can be expended into many sinks, only two of which, directed electromagnetic kinetic power and directed electrothermal kinetic power, are useful for propulsion. Understanding and quantifying these disparate processes are essential to improving the efficiency of these devices. Since an empirical approach alone is not generally conducive to obtaining such detailed information on these physical processes, numerical simulations are valuable tools in plasma thruster research. Given the dearth of high-power test facilities, simulations can be valuable aides to research for high-power plasma propulsion, by reducing the need for expensive, and sometimes unviable, experimental parametric studies.

The goal of this work is to develop a robust numerical solver for the simulation of plasma devices in which the flows can be treated as a fluid, such as magnetoplasmadynamic thrusters (MPDT) described in References [1, 4, 5], and apply it to investigate the role of physical processes in these devices.

1.2. Existing work

The importance of numerical simulations in advancing plasma thruster research was realized early in its history. Some notable efforts in propulsive plasma flow simulation are summarized here.

Kimura *et al.* [9] and Fujiwara [10], started developing single-temperature, 2-D models on simple geometries, and have continued to make improvements to their models. Currently, the efforts of Fujiwara *et al.* [11] are directed at studying critical phenomena in magnetoplasmadynamic thrusters (MPDT), using multitemperature models. Caldo and Choueiri [12] developed a two-temperature model to study the effects of anomalous transport, described in Reference [13], on MPDT flows. The effort by LaPointe [14] focused on studying the effects of geometry on performance. Martinez-Sanchez *et al.* [15, 16] have developed multi-temperature axisymmetric numerical models to study various aspects of the flow such as anode voltage drops and the role of viscous effects. Turchi *et al.* [17] use MACH2, an unsteady MHD solver developed for high-power plasma gun simulation, to model pulsed plasma thrusters (PPTs) and MPDTs in many geometries. MACH3 [18], the next generation of MACH2, is also used to simulate possible 3-D effects in specific situations. The most persistent effort so far has been that of Auweter-Kurtz *et al.* [20, 21] at University of Stuttgart, who have been developing numerical models for MPDTs for almost two decades. Detailed models for many transport processes and multiple levels of ionization have been incorporated into their governing equations, which are solved on unstructured adaptive grids.

1.3. Current approach

Despite the efforts described above, there remains a need for accurate and robust numerical schemes to simulate propulsive plasma flows. In particular, improvements are required in three aspects:

1. Some of the above-mentioned codes exhibit numerical instabilities at high current levels. Many electromagnetic thrusters, especially MPDTs, perform better at higher currents, and many of the important research questions, such as performance limiting phenomena, tend to also occur at higher current levels, or more specifically at $J^2/\dot{m} \geqslant 40.0\,\mathrm{kA}^2/\mathrm{g/s}$, where J is the

total current, and $\dot{m}$ is the mass flow rate. Therefore, it is important to be able to simulate at the required values of $J^2/\dot{m}$.

A probable explanation for these instabilities is the failure to solve the magnetic field evolution self-consistently with the flow (since separate solvers for the fluid and field equations were used). For highly resistive flows, the time scale for resistive diffusion of the magnetic field is orders of magnitude smaller than that of convection. However, in MPD flows it is common to have resistivities of $\mathcal{O}(10^{-4})\,\Omega\,\mathrm{m}$. In such situations, these time scales are not very disparate, and there is a strong coupling between the flow and the magnetic field. The corresponding magnetic Reynolds' numbers indicate that both convective and resistive diffusion of the magnetic field are important. Therefore, the full set of equations describing the flow field and magnetic field evolution has to be computed self-consistently, by including both the magnetic field and the conserved fluid quantities together, in the vector of quantities to be computed, by the same solver, as in Equation (1).

An important feature of the MHD formalism is the multitude of waves it permits to exist. The non-linear coupling of these waves play an important role in determining physical phenomena and in computing the solution, as explained in Reference [22]. Solving Maxwell's equations consistently with the equations of compressible gasdynamics naturally produces waves physically associated with the problem, such as Alfvèn and magnetosonic waves, as eigenvalues. Such a formulation is thus suitable for handling MHD waves and shocks.

2. Some of the earlier efforts [12, 19] have experienced problems conserving mass, momentum and energy. A conservative formulation of the governing equations ensures that these quantities are indeed conserved. Such a formulation also facilitates the application of boundary conditions, since the fluxes are the only quantities to be specified at the boundaries. From the perspective of numerical solution, it can be shown that conservative formulation is necessary for accurately capturing discontinuities.

3. As also noted in Reference [16], none of the existing models (with the exception of the recent work in Reference [21]) take advantage of the developments in the techniques for numerical solution of Euler and Navier–Stokes equations.

Each of the problems mentioned above can be overcome, respectively, by adapting the following approach:

1. Treat the flow and magnetic field equations in a self-consistent manner.
2. Formulate the governing equations in a conservative form.
3. Use characteristics-splitting techniques satisfying Rankine–Hugoniot relations, combined with anti-diffusion to increase accuracy. These techniques can capture shocks and other strong gradients in a non-oscillatory manner, and can have good spatial accuracy in smooth regions of the flow.

The solver developed based on these principles will be described in the following sections.

1.4. Outline

The MHD equations, which this scheme attempts to solve, are described in Section 2. The issues in obtaining a numerical solution are discussed in Section 3. A new characteristics-splitting technique for the solution of the ideal MHD equations is described and validated in Section 4. The capability of this scheme to simulate real magnetoplasmadynamic flows is briefly demonstrated in Section 5.3. Details of the physical results from the simulation

of MPDT flow will be the subject of a future paper, and we will focus here on the solver only.

2. MHD EQUATIONS

The solver developed in this work can be illustrated with the simple flow problem of a fully ionized, quasi-neutral plasma in thermal equilibrium under conditions for which the continuum treatment is valid. Subsequent physical models can be added as deemed appropriate, without significant changes to the underlying numerical building blocks of the solver. The governing equations for this problem can be written in the form

$$\frac{\partial}{\partial t}\begin{bmatrix}\rho\\ \rho\mathbf{u}\\ \mathbf{B}\\ \mathscr{E}\end{bmatrix}+\nabla\cdot\begin{bmatrix}\rho\mathbf{u}\\ \rho\mathbf{u}\mathbf{u}+\bar{\bar{p}}-\bar{\bar{\mathscr{B}}}_{\mathrm{M}}\\ \mathbf{u}\mathbf{B}-\mathbf{B}\mathbf{u}\\ (\mathscr{E}+p)\mathbf{u}-\bar{\bar{\mathscr{B}}}_{\mathrm{M}}\cdot\mathbf{u}\end{bmatrix}=\nabla\cdot\begin{bmatrix}0\\ 0\\ \bar{\bar{E}}_{\mathrm{res}}\\ \mathbf{q}\end{bmatrix} \tag{1}$$

The continuity equation does not have any source or sink terms because this model assumes complete ionization and no recombination.

The momentum equation contains the electromagnetic body force per unit volume, $\mathbf{j}\times\mathbf{B}$, written as the divergence of the Maxwell stress tensor $\bar{\bar{\mathscr{B}}}_{\mathrm{M}}$, as described in Reference [1]. Here, $\bar{\bar{p}}$ is the isotropic thermodynamic pressure tensor. Currently, viscous effects are neglected in this work.

In Faraday's law, the convective diffusion of the magnetic field, which is the contribution of the back EMF, is written as a divergence of the antisymmetric tensor $\mathbf{u}\mathbf{B}-\mathbf{B}\mathbf{u}$. The resistive diffusion appears as divergence of the resistive diffusion tensor, $\bar{\bar{E}}_{\mathrm{res}}$, defined such that [23],

$$\nabla\cdot\bar{\bar{E}}_{\mathrm{res}}=-\nabla\times\left[\bar{\bar{\eta}}\cdot\mathbf{j}\right] \tag{2}$$

where $\bar{\bar{\eta}}$ is the full resistivity tensor, which includes the Hall effect.

The energy equation is written in terms of the energy density (energy per unit volume), $\mathscr{E}$, whose components are the internal energy, kinetic energy and the energy in the magnetic field

$$\mathscr{E}=\frac{p}{\gamma-1}+\frac{1}{2}\rho\mathbf{u}\cdot\mathbf{u}+\frac{\mathbf{B}\cdot\mathbf{B}}{2\mu_0} \tag{3}$$

Here, the effects of deposition of energy into internal modes, and thus of a real caloric equation of state, enter through the variation of γ.

Apart from the familiar convective flux of energy, $(\mathscr{E}+p)\mathbf{u}$, the other terms are the energy invested in electromagnetic acceleration, $\bar{\bar{\mathscr{B}}}_{\mathrm{M}}\cdot\mathbf{u}$, and the energy sources/sinks due to viscous heating, Ohmic heating, and thermal conduction,

$$\nabla\cdot\mathbf{q}=\nabla\cdot\left[\bar{\bar{\tau}}_{\mathrm{vis}}\cdot\mathbf{u}+\frac{\mathbf{B}\times\mathbf{E}'}{\mu_0}+\bar{\bar{k}}_{\mathrm{th}}\cdot\nabla T\right] \tag{4}$$

where $\mathbf{E}'=\mathbf{E}+\mathbf{u}\times\mathbf{B}$, is the electric field in the plasma reference frame, and $\bar{\bar{k}}_{\mathrm{th}}$ is the coefficient of thermal conduction.

Under some physical conditions, when the magnetic pressure is several orders of magnitude larger than thermodynamic pressure, the conservation form of the energy equation may not be suitable. In these cases, since the thermodynamic pressure, p, is calculated by subtracting one large number ($B^2/2\mu_0$) from another ($\mathscr{E}$), the associated errors could be large. However, for the conditions that are of interest to plasma propulsion, the magnetic pressure is seldom two orders of magnitude greater than thermodynamic pressure. Thus, the conservation form of the energy equation is numerically suitable here.

Since the physical dissipation is written in the divergence form, the entire set of equations can be written in the form

$$\frac{\partial \mathbf{U}}{\partial t} + \nabla \cdot \mathscr{F}_{\text{conv}} = \nabla \cdot \mathscr{F}_{\text{diff}} \tag{5}$$

where $\mathscr{F}_{\text{conv}}$ is the convective flux tensor and represents the hyperbolic part of the problem and $\mathscr{F}_{\text{diff}}$, the dissipative flux tensor, represents the parabolic part of the problem.

Though Maxwell's equations prescribe that $\nabla \cdot \mathbf{B} \equiv 0$, it is often not true numerically. Strictly, these terms containing $\nabla \cdot \mathbf{B}$ appear on the right-hand side of Equation (1) as

$$\mathbf{S}_{\nabla \cdot \mathbf{B}} = (\nabla \cdot \mathbf{B}) \left[0, \frac{\mathbf{B}}{\mu_0}, \mathbf{u}, \frac{\mathbf{B}}{\mu_0} \cdot \mathbf{u}\right]^{\mathrm{T}} \tag{6}$$

The treatment of the $\nabla \cdot \mathbf{B}$ terms are important, since they could be a cause of numerical instabilities, as explained in Reference [24]. The present work uses the technique of Powell [25] to absorb these terms into the eigensystem, without affecting the conservation form of equation (5). Then, any artificial source is convected away as

$$\frac{\partial}{\partial t}(\nabla \cdot \mathbf{B}) + \nabla \cdot (\mathbf{u} \nabla \cdot \mathbf{B}) = 0 \tag{7}$$

Moreover, for self-induced field MPDTs in a coaxial geometry, the magnetic field is purely azimuthal ($B_r = B_z = 0$). Thus, under the assumption of axial symmetry,

$$\nabla \cdot \mathbf{B} = \frac{1}{r} \frac{\partial B_\theta}{\partial \theta} \equiv 0 \tag{8}$$

Therefore, the zero divergence of magnetic field in the solution is always ensured in the simulation of MPDT flows.

3. NUMERICAL SOLUTION

The emphasis of this paper is on the numerical techniques for the hyperbolic nature of the convective part of the problem. This is because the goal of this work is to simulate problems in plasma propulsion, consequently computing the flow is the most important part. More importantly, it is this part of the problem that has required improvements. The dissipative part of the problem, which is responsible for adding a parabolic nature to the governing equations, is relatively well understood. However, as explained in Section 1.2, there is strong coupling between the hyperbolic and the parabolic parts of the problem. This coupling raises important issues in spatial as well as temporal discretization, which will be discussed in this section.

3.1. Mesh system

Before delving into the details of numerical solution, a choice of mesh system has to be made. For the cylindrical co-ordinate system that is most suitable for the study of many plasma thrusters, the easiest choice is to use structured orthogonal grids where the finite volumes are concentric shells. Apart from their simplicity, they are also computationally inexpensive. However, they impose a limitation on the variety and complexity of geometries that can be modeled.

The use of unstructured grids to simulate plasma thrusters has gained some popularity [20, 21]. Though the obvious advantage is the freedom to specify an arbitrary geometry, there are some disadvantages that may not be immediately apparent. Unstructured grids are computationally expensive and there are problems in extending higher order accurate schemes to them. Since precise control of geometry may not be as critical to the design of plasma thrusters as it is to, say aircraft design, the use of unstructured grids may not be as crucial. A good settlement of this issue would be to use body-fitted meshes, and maintain the use of higher order accurate schemes. Since the focus of this paper is on the solver and its validation, and not on the details of the simulation of complex flows, we adopt a standard structured orthogonal grid system.

The variables to be computed, given by $\mathbf{U}$ in Equation (5), can be stored either in the vertices of the cells, or in the centre of the cells [29]. In the former, the variables will coincide with the boundary, and they will be specified as boundary conditions. In the latter, the faces of the cells will be aligned with the walls, and the fluxes of these variables will be specified as boundary conditions. While solving the conservative formulation, it is preferable to choose the cell-centred scheme since specifying the fluxes is more compatible with the governing equations.

3.2. Spatial discretization

The numerical solution of the set of hyperbolic equations is based on techniques that are extensively used in computational fluid dynamics. The principles underlying the design of non-oscillatory discretization schemes for compressible flows have been well established over the past decade. There are two important issues in the design of discretization schemes:

- estimating the numerical flux through cell boundaries, and accounting for waves propagating at different speeds, and possibly in different directions,
- obtaining non-oscillatory solutions and capturing discontinuities with sufficient accuracy.

The numerical scheme used in this work is derived from research based on the pioneering work of Godunov [30, 31]. The characteristics-splitting technique, which will be described later, was first developed [33, 34] to solve problems in compressible fluid dynamics, and has been proven to work reliably in the solution of Euler equations.

The most popular check for the stability and convergence of a nonlinear set of equations is the total variation diminishing (TVD) principle [35]. A practical limitation of the TVD condition is that its extension to multidimensional problems does not provide a satisfactory measure of numerical oscillations [36]. The concept of local extremum diminishing (LED) schemes, developed by Jameson [36], can be extended to multiple dimensions, and ensures that there are no unbounded local oscillations. It has been shown [36] that TVD is in fact a 1-D special case of the LED framework. These schemes can be combined with flux limited

anti-diffusion to provide higher-order accuracy in smooth regions of the flow. These concepts are explained in Section 4.

Numerical methods for parabolic problems are relatively commonplace. The equations dictate that the numerical scheme should be second-order accurate in space. In the framework used here, this implies that the first derivatives of variables are to be known across the cell faces. Standard explicit centered spatial differences for the parabolic terms is used in this work.

3.3. Temporal discretization

Unlike in fluid mechanics, the equations of MHD allow many different types of waves to exist. Even though physically the flow velocity is one of the sought quantities of most interest to propulsion, numerically the velocity of the fastest wave is what determines the time-step constraints. In plasmas of propulsion interest, the fluid velocity is $\mathcal{O}(10^4)$ m/s. For a quasineutral plasma in which the number density of charged particles is $\mathcal{O}(10^{21})$ /m^3 and thermodynamic pressures of $\mathcal{O}(10^{-1})$ Torr and magnetic pressure of $\mathcal{O}(10^{1})$ Torr, the fast magnetosonic wave speed is typically of the same order of magnitude as the flow velocity. This indicates that an explicit time marching scheme is suitable for the ideal MHD case. For dissipative MHD the choice of time step depends on the relative magnitude of dissipative time scales and convective time scales, as explained further down in this section. From the Courant–Friedrichs–Lewyor (CFL) criterion [35], the time step for the ideal MHD problem would be $\mathcal{O}(10^{-8}$–$10^{-9})$ s.

A multistage scheme can be chosen to march forward in time. Writing Equation (1) as

$$\frac{\mathrm{d}\mathbf{U}}{\mathrm{d}t} + \mathscr{F}(\mathbf{U}) = 0 \tag{9}$$

where $\mathscr{F}(\mathbf{U})$ represents the sum of all the fluxes, the multistage scheme can be written as

$$\begin{aligned}
\mathbf{U}^1 &= \mathbf{U}^n - \alpha_1 \Delta t \mathscr{F}(\mathbf{U}^n) \\
\mathbf{U}^2 &= \mathbf{U}^n - \alpha_2 \Delta t \mathscr{F}(\mathbf{U}^1) \\
\mathbf{U}^3 &= \mathbf{U}^n - \alpha_3 \Delta t \mathscr{F}(\mathbf{U}^2) \\
\mathbf{U}^4 &= \mathbf{U}^n - \alpha_4 \Delta t \mathscr{F}(\mathbf{U}^3) \\
\mathbf{U}^{n+1} &= \mathbf{U}^4
\end{aligned} \tag{10}$$

The values of α_1, α_2, α_3 and α_4 correspond to maximum time accuracy, and were obtained from Reference [28] to be $\alpha_1 = 0.1084$, $\alpha_2 = 0.2602$, $\alpha_3 = 0.5052$ and $\alpha_4 = 1.0$.

Physical dissipation brings in different characteristic time scales into the problem. They are (for a typical mesh dimension of $\sim$1 mm):

Viscous diffusion: $= \rho \Delta r^2 / \mu_{\mathrm{visc}} \sim 10^{-9}$–$10^{-10}$ s

Magnetic diffusion: $= \mu_0 \Delta r^2 / \eta \sim 10^{-10}$–$10^{-11}$ s

Heat conduction: $= n_{\mathrm{e}} k_{\mathrm{B}} \Delta r^2 / \kappa_{\mathrm{th}} \sim 10^{-9}$–$10^{-11}$ s

A suitable choice of time-marching scheme can be made depending upon where the time scales lie in the particular case of interest. If the disparity between the convective and dissipative time

scales is $\sim\mathcal{O}(10\text{–}100)$, then evaluating the convective fluxes at the time scales of dissipative fluxes would be prohibitively expensive. In order to side step this difficulty, a fractional time-stepping scheme may be useful. In this method, the convective fluxes are updated only after N dissipative time steps, such that $N\Delta t$ is still less than the convective time scale. We have worked with values of N ranging from 10 to 50, depending on the plasma conditions.

4. SOLUTION OF THE IDEAL MHD EQUATIONS

4.1. Characteristics-splitting method

Any time-dependent conservation law, such as Equation (1), can be written in a general form

$$\frac{\mathrm{d}\mathbf{U}_j}{\mathrm{d}t} = \sum_{j\neq k} C_{j,k}(\mathbf{U}_k - \mathbf{U}_j) \tag{11}$$

If the numerical scheme has a compact stencil in which the value of $\mathbf{U}$ at a point is directly dependent only on its nearest neighbours, and if the coefficients are all non-negative, then

$$C_{j,k} = \begin{cases} \geqslant 0, & k = j\pm 1 \\ = 0, & \text{else} \end{cases} \tag{12}$$

If $\mathbf{U}_j$ is a local maximum, then, $(\mathbf{U}_k - \mathbf{U}_j) \leqslant 0$, causing $\mathrm{d}\mathbf{U}_j/\mathrm{d}t \leqslant 0$. Conversely, if $\mathbf{U}_j$ is a local minimum, then, $(\mathbf{U}_k - \mathbf{U}_j) \geqslant 0$, causing $\mathrm{d}\mathbf{U}_j/\mathrm{d}t \geqslant 0$. In other words, this scheme is local extremum diminishing. Apart from ensuring that there are no local numerical oscillations, a scheme built on these conditions can be easily extended to multi dimensions, unlike the case of the TVD concept.

It has been shown [36] that schemes built on obtaining information from the upwind part of a characteristic satisfy positivity constraints (Equation (12)) and are thus stable for solving equations of hyperbolic nature, such as the ideal MHD equations. This concept is used in developing the numerical scheme used in this work.

The method can be explained using Equation (1) in one-spatial dimension,

$$\frac{\mathrm{d}\mathbf{U}_j}{\mathrm{d}t} + \frac{\mathbf{Hz}_{j+1/2} - \mathbf{Hz}_{j-1/2}}{\Delta z} = 0 \tag{13}$$

where $\mathbf{U}$ is the vector of conserved variables, $\mathbf{Hz}$ is the approximation of flux in the $\hat{z}$ direction.

The true flux, obtained from equation (1), in the $\hat{z}$ direction can be split as

$$\mathbf{Fz}(\mathbf{U}) = \mathbf{Fz}(\mathbf{U})^+ + \mathbf{Fz}(\mathbf{U})^- \tag{14}$$

where the eigenvalues of $\mathrm{d}\mathbf{Fz}^+/\mathrm{d}\mathbf{U}$ are all positive or zero, and the eigenvalues of $\mathrm{d}\mathbf{Fz}^-/\mathrm{d}\mathbf{U}$ are all negative or zero. Then, the approximation of flux is estimated as

$$\mathbf{Hz}_{j+1/2} = \mathbf{Fz}_j^+ + \mathbf{Fz}_{j+1}^-$$

This method of splitting fluxes was originally developed by Boris and Book [32] for the solution of Euler equations. Using Equation (14), this can be rewritten as

$$\mathbf{Hz}_{j+1/2} = \tfrac{1}{2}(\mathbf{Fz}_j + \mathbf{Fz}_{j+1}) - \mathbf{Dz}_{j+1/2}$$

where

$$\mathbf{Dz}_{j+1/2} = \tfrac{1}{2}[\{\mathbf{Fz}^{+}_{j+1} - \mathbf{Fz}^{+}_{j}\} - \{\mathbf{Fz}^{-}_{j+1} - \mathbf{Fz}^{-}_{j}\}] \tag{15}$$

There still remains a question of how $\mathbf{Fz}^{+}$ and $\mathbf{Fz}^{-}$ can be evaluated. This evaluation is possible if there is a matrix $\mathbf{A}$, such that

$$\mathbf{Fz}_{j+1} - \mathbf{Fz}_{j} = \mathbf{A} \cdot (\mathbf{U}_{j+1} - \mathbf{U}_{j}) \tag{16}$$

Note that, in the case the points $j+1$ and j are on opposite sides of a discontinuity, Equation (16) indicates that this scheme satisfies the Rankine–Hugoniot jump conditions exactly, if such a matrix $\mathbf{A}$ exists.

For a hyperbolic system of equations, $\mathbf{A}$ can be diagonalized as

$$\mathbf{A} \equiv \mathbf{R}\Lambda\mathbf{R}^{-1} \tag{17}$$

where $\mathbf{R}$ (given in the appendix) contains the right eigenvectors of $\mathbf{A}$ as its columns, and $\mathbf{R}^{-1}$ (also given in the appendix) contains the left eigenvectors of $\mathbf{A}$ as its rows. Λ is the diagonal matrix of eigenvalues of $\mathbf{A}$ (given in the appendix). Since Λ can be easily split as, $\Lambda = \Lambda^{+} + \Lambda^{-}$, using Equation (17), $\mathbf{A}$ can be split. Thus if there exists an $\mathbf{A}$ such that Equation (16) is true, then $\mathbf{F}$ can be split. For the Euler equations, this matrix was derived by Roe [33, 34]. There have been efforts by Cargo [37] and Powell [26] to derive such matrices for MHD equations. The literature [38] suggests that various forms of averaged matrices work satisfactorily.

From Godunov's theorem [30], it is evident that the scheme can only be first order accurate. However, away from the discontinuities, the spatial accuracy of the scheme can be improved by including flux-limited anti-diffusion, $\mathbf{Lz}$, as described in Reference [36]:

$$\mathbf{Dz}_{j+1/2} = \tfrac{1}{2}|\mathbf{A}|[\Delta\mathbf{U}_{j+1/2} - \mathbf{Lz}(\Delta\mathbf{U}_{j+3/2}, \Delta\mathbf{U}_{j-1/2})] \tag{18}$$

Similar equations can be written for the corresponding terms in the $\hat{r}$ direction.

An alternative to characteristics splitting for solving conservation form of the equations is to use scalar diffusion. In this formalism, the numerical diffusion is

$$\mathbf{Dz}_{j+1/2} = \tfrac{1}{2}|\lambda|_{\max}\, \Delta\mathbf{U}_{j+1/2} \tag{19}$$

Because of their low computational cost, schemes such as Equation (19) have been successfully adapted for many applications such as aircraft design. However, since these schemes tend to artificially smooth out the solution [36], Equation (19) was only used in our work for comparison with Equation (18).

5. VERIFICATION OF THE SCHEME

5.1. Unsteady case

The test problem chosen to validate the characteristics-splitting scheme for the ideal MHD solver was of the classical Riemann type, which consists of a single jump discontinuity in an

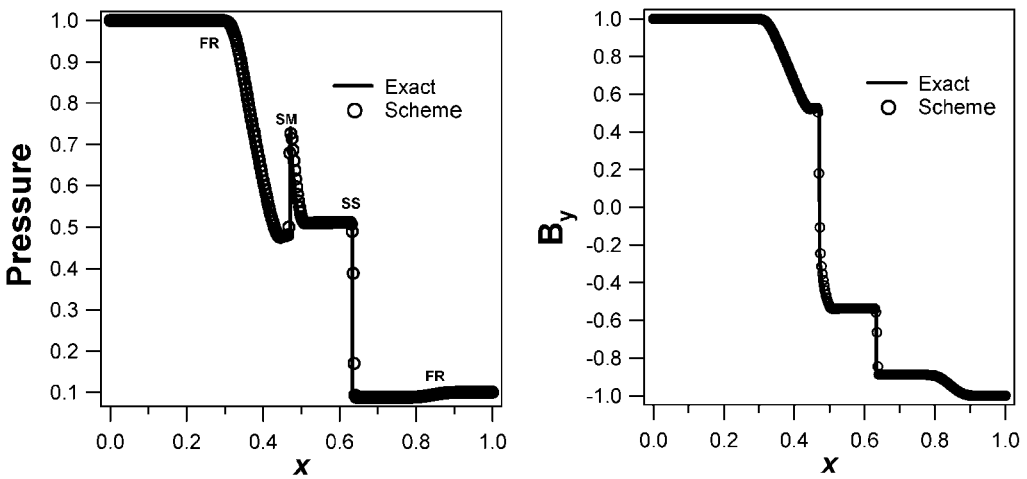

Figure 1. Exact and numerical solutions of the magnetic field and pressure profiles for the Riemann problem.

otherwise smooth initial condition. In 1-D the problem is

$$\mathbf{U}(x,0) = \begin{cases} \mathbf{U}_{\mathrm{L}} & \text{if } x < \frac{L}{2} \\ \mathbf{U}_{\mathrm{R}} & \text{if } x \geqslant \frac{L}{2} \end{cases} \tag{20}$$

The Riemann problem was chosen because it is one of the very few that have an analytical solution. This problem provides an excellent illustration of the wave solution to the problem inherent to the equations. The solution to the Riemann problem is useful to verify the capturing of both smooth waves (characteristics) as well as non-smooth waves (shocks).

The initial states used were very similar to the Sod problem [39] for the Euler equations, and were first used by Brio and Wu [40] for the validation of MHD solvers. They were

$$\begin{aligned} &\textit{Left}: \ \left[\rho = 1.0, V_x = 0.0, V_y = 0.0, V_z = 0.0, B_x = \tfrac{3}{4}, B_y = 1.0, B_z = 0.0, p = 1.0\right]^{\mathrm{T}} \\ &\textit{Right}: \ \left[\rho = \tfrac{1}{8}, V_x = 0.0, V_y = 0.0, V_z = 0.0, B_x = \tfrac{3}{4}, B_y = -1.0, B_z = 0.0, p = \tfrac{1}{10}\right]^{\mathrm{T}} \end{aligned} \tag{21}$$

The solution was computed at a dimensionless time (defined in Reference [40], based on the fast magnetosonic speed and the grid dimension) of $\tau = 0.1$, with the initial conditions described above. The solutions for the magnetic field and pressure profiles, with 400 points in the spatial dimension, are presented in Figure 1. The number of points in the domain, and the time τ were chosen to allow comparisons to other works, such as Reference [25].

In these figures, the fast rarefaction (FR) wave can be seen on the far right and the far left, as it is the fastest of wave in the problem. The slow shock (SS) and the compound wave (SM) have speeds less than that of the FR wave.

As shown in these figures, the scheme successfully captures the time-dependent discontinuities.

5.2. Steady-state case

In order to simulate steady-state MHD flows, this solver can be used to solve the unsteady equation to steady state. Then, an important question is whether it remains in that steady state. To answer this question, a test problem was chosen, whose equilibrium solution is known analytically. This equilibrium solution is given as the initial condition for the solver. After marching several hundreds or thousands of time steps, a check is performed to see if the variables have changed from the initial conditions.

The test problem chosen for this simulation was the Taylor State [41] configuration. Under certain conditions, described in Reference [41], when a bounded ideal plasma is allowed to evolve, it will move quickly and dissipate energy before coming to rest. This stable equilibrium configuration can be analytically found using the minimum energy principle, and is of the form

$$\nabla \times \mathbf{B} = \lambda \mathbf{B} \tag{22}$$

where λ is an eigenvalue.

Since the current is parallel to the magnetic field, the $\mathbf{j} \times \mathbf{B}$ body force is identically zero. Furthermore, if there are no thermodynamic pressure gradients, the plasma is in a state of force-free equilibrium. For an axisymmetric geometry, the resulting magnetic field profile is

$$B_\theta = B_0 J_1(\lambda r), \quad B_z = B_0 J_0(\lambda r) \tag{23}$$

where B_0 is a constant amplitude, J_0 and J_1 are Bessel functions of the first kind, of orders 0 and 1, respectively.

For a Cartesian grid of dimensions $L_x \times L_z$, with symmetry along the $\hat{y}$ direction, the magnetic field distribution satisfying Equation (22) is

$$\begin{aligned} B_x &= -\frac{B_0}{\sqrt{2}} \sin\left(\frac{m\pi x}{L_x}\right) \cos\left(\frac{n\pi z}{L_z}\right) \\ B_y &= B_0 \sin\left(\frac{m\pi x}{L_x}\right) \sin\left(\frac{n\pi z}{L_z}\right) \\ B_z &= \frac{B_0}{\sqrt{2}} \cos\left(\frac{m\pi x}{L_x}\right) \sin\left(\frac{n\pi z}{L_z}\right) \end{aligned} \tag{24}$$

where m and n are eigenvalues. The boundary conditions for this test case were: all components of velocity are set to zero at the boundaries, the pressure is maintained to be the same uniform value specified for the entire domain, and the magnetic field components at the boundary were kept unchanged from the initial distribution.

With the initial conditions specified above, the code was run for 10^4 time steps on a 100×100 grid. At the end, the solution had deviated from equilibrium by less than 0.5 per cent. The results from the code for B_x given in Equation (24) are compared with the exact solution in Figure 2. Thus the *property of linearity preservation* has been successfully verified for this solver.

5.3. Current density pattern in a MPDT

The test cases described above were intended to validate the new characteristics splitting scheme, which was developed to calculate the convective part of the MHD equations. Therefore, a vastly simplified ideal MHD system was considered. Specifically, the equations

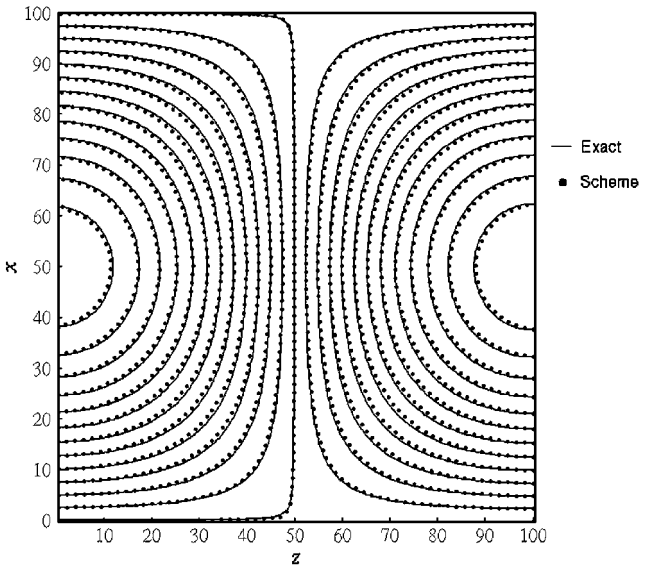

Figure 2. Exact and numerical solution of magnetic field in the Taylor configuration.

described above assume a fully ionized plasma, with ideal equation of state, in thermal equilibrium, with no dissipative effects. However, the physical processes in propulsive plasmas are far more complex.

As a first improvement, the effects of resistive diffusion, Hall effect, and gradient drifts along with electron and ion thermal conduction, described in Section 2, had to be included. Furthermore, the thermal non-equilibrium between the electrons and the ions had to be accounted for. This required additional species energy equations to be solved concurrently with Equation (1). For the conditions of interest to propulsion, the deviation from the ideal equation of state is strong, and therefore the ratio of specific heats, and the nonlinear relationship between density pressure and temperature had to be computed. Anomalous transport effects, described in Reference [13], due to the momentum exchange between particles and waves, also had to be accounted for. Furthermore, a multilevel equilibrium ionization model [21] to compute the densities of electrons and ions of various stages of ionization was incorporated into the code. It is important to note that all these effects were included without any changes to the underlying scheme. Since the focus of the present paper is on the numerical scheme only, we refer the interested reader to Reference [8] for all the details regarding the physical models, transport coefficients, initial and boundary conditions.

To illustrate the utility of this solver, the flow field of a real MPDT, operating under nominal conditions, was simulated. In the case chosen, argon plasma at a mass flow rate of 6.0 g/s was flowing in the channel, with 15.0 kA of discharge current. The calculated contours of enclosed current at steady state are shown in Figure 3. All the current is downstream of the backplate, and there is 2500 A of current flowing between each contour. In ideal MHD, magnetic field and therefore current lines, which are lines of constant rB_θ, would be convected to the exit. However, due to the presence of resistivity, the current lines remain in the channel.

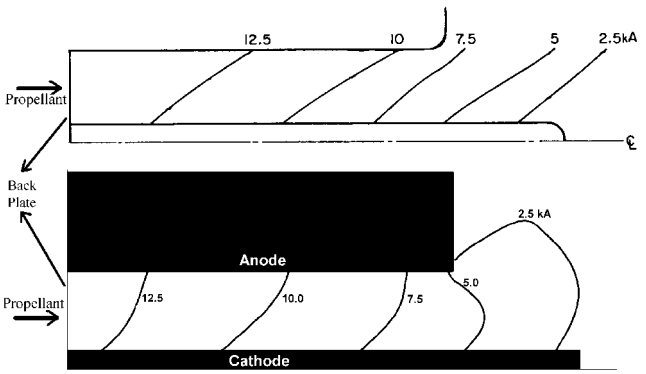

Figure 3. Measured (top) and calculated (bottom) enclosed current contours.

It is also apparent that many current lines inside the thruster are not vertical. This is due to a combination of the Hall effect that causes current conduction in the axial direction, and convective effects.

On comparison with experimental data, it was found that the results of the simulation yielded realistic values and profiles for the plasma parameters of interest [8].

6. CONCLUDING REMARKS

A new solver to accurately compute plasma flows of interest to propulsion has been developed and validated. The characteristics-splitting technique is used to capture discontinuities monotonically. Flux-limited anti-diffusion to improve spatial accuracy away from discontinuities, and a multistage time-stepping scheme to improve temporal accuracy are used in this numerical method. Further improvements to the physical model were added without any changes to the underlying scheme. This solver has demonstrated the capability to produce realistic simulation of thruster flow fields for the operating conditions considered.

APPENDIX A. EIGENSYSTEM OF MHD

Alfvèn speeds

$$C_{\mathrm{A};r,\theta,z} = \frac{B_{r,\theta,z}}{\sqrt{\mu_0 \rho}}$$

Sonic speed

$$a = \sqrt{\frac{\gamma p}{\rho}}$$

Normalization coefficients (based on the work in References [26, 27])

$$\beta_{r;\theta,z} = \frac{C_{\mathrm{A};\theta,z}}{\sqrt{C_{\mathrm{A};\theta}^2 + C_{\mathrm{A};z}^2}}, \quad \alpha_{r;f,s} = \sqrt{\pm \frac{a^2 C_{\mathrm{S,F};r}^2}{C_{\mathrm{F};r}^2 - C_{\mathrm{S};r}^2}}$$

$$\beta_{z;r,\theta} = \frac{C_{\mathrm{A};r,\theta}}{\sqrt{C_{\mathrm{A};r}^2 + C_{\mathrm{A};\theta}^2}}, \quad \alpha_{z;f,s} = \sqrt{\pm \frac{a^2 C_{\mathrm{S,F};z}^2}{C_{\mathrm{F};z}^2 - C_{\mathrm{S};z}^2}}$$

Fast and slow magnetosonic waves

$$C_{\mathrm{F,S};r}^2 = \frac{1}{2}\left[\left(\frac{\mathbf{B}\cdot\mathbf{B}}{\mu_0\rho} + a^2\right) \pm \sqrt{\left(\frac{\mathbf{B}\cdot\mathbf{B}}{\mu_0\rho} + a^2\right)^2 - (4a^2 C_{\mathrm{A};r}^2)}\right]$$

$$C_{\mathrm{F,S};z}^2 = \frac{1}{2}\left[\left(\frac{\mathbf{B}\cdot\mathbf{B}}{\mu_0\rho} + a^2\right) \pm \sqrt{\left(\frac{\mathbf{B}\cdot\mathbf{B}}{\mu_0\rho} + a^2\right)^2 - (4a^2 C_{\mathrm{A};z}^2)}\right]$$

The Jacobian of transformation between primitive and conservation variables

$$\frac{\mathrm{d}\mathbf{U}}{\mathrm{d}\mathbf{W}} = \begin{bmatrix} 1 & 0 & 0 & 0 & 0 & 0 & 0 & \\ u & \rho & 0 & 0 & 0 & 0 & 0 & 0 \\ v & 0 & \rho & 0 & 0 & 0 & 0 & 0 \\ w & 0 & 0 & \rho & 0 & 0 & 0 & 0 \\ 0 & 0 & 0 & 0 & 1 & 0 & 0 & 0 \\ 0 & 0 & 0 & 0 & 0 & 1 & 0 & 0 \\ 0 & 0 & 0 & 0 & 0 & 0 & 1 & 0 \\ \dfrac{\mathbf{u}\cdot\mathbf{u}}{2} & \rho u & \rho v & \rho w & \dfrac{B_x}{\mu_0} & \dfrac{B_y}{\mu_0} & \dfrac{B_z}{\mu_0} & \dfrac{1}{\gamma - 1} \end{bmatrix}$$

A.1. $\hat{r}$ direction

A.1.1. Eigenvalues (in non-decreasing order)

$$[u - C_{\mathrm{F};r}, u - C_{\mathrm{A};r}, u - C_{\mathrm{S};r}, u, u, u + C_{\mathrm{S};r}, u + C_{\mathrm{A};r}, u + C_{\mathrm{F};r}] \tag{A1}$$

A.1.2. Ortho-normalized eigenvectors

$$L1_r = \left[0, \frac{-\alpha_{r;f} C_{\mathrm{F};r}}{2a^2}, \frac{\alpha_{r;s} C_{\mathrm{S};r} \beta_{r;\theta}\,\mathrm{Sgn}[B_r]}{2a^2}, \frac{\alpha_{r;s} C_{\mathrm{S};r} \beta_{r;z}\,\mathrm{Sgn}[B_r]}{2a^2}, 0,\right.$$

$$\left.\frac{\alpha_{r;s}\beta_{r;\theta}}{2a\sqrt{\mu_0\rho}}, \frac{\alpha_{r;s}\beta_{r;z}}{2a\sqrt{\mu_0\rho}}, \frac{\alpha_{r;f}}{2\rho a^2}\right]$$

$$L2_r = \left[0, 0, -\frac{\beta_{r;z}}{\sqrt{2}}, \frac{\beta_{r;\theta}}{\sqrt{2}}, 0, -\frac{\beta_{r;z}}{\sqrt{2\mu_0\rho}}, \frac{\beta_{r;\theta}}{\sqrt{2\mu_0\rho}}, 0\right]$$

$$L3_r = \left[0, \frac{-\alpha_{r;s}C_{S;r}}{2a^2}, \frac{-\alpha_{r;f}C_{F;r}\beta_{r;\theta}\,\mathrm{Sgn}[B_r]}{2a^2}, \frac{-\alpha_{r;f}C_{F;r}\beta_{r;z}\,\mathrm{Sgn}[B_r]}{2a^2}, 0,\right.$$
$$\left.\frac{-\alpha_{r;f}\beta_{r;\theta}}{2a\sqrt{\mu_0\rho}}, \frac{-\alpha_{r;f}\beta_{r;z}}{2a\sqrt{\mu_0\rho}}, \frac{\alpha_{r;f}}{2\rho a^2}\right]$$

$$L4_r = [1, 0, 0, 0, 0, 0, 0, -1/a^2]$$

$$L5_r = [0, 0, 0, 0, 1, 0, 0, 0]$$

$$L6_r = \left[0, \frac{\alpha_{r;s}C_{S;r}}{2a^2}, \frac{\alpha_{r;f}C_{F;r}\beta_{r;\theta}\,\mathrm{Sgn}[B_r]}{2a^2}, \frac{\alpha_{r;f}C_{F;r}\beta_{r;z}\,\mathrm{Sgn}[B_r]}{2a^2}, 0,\right.$$
$$\left.\frac{-\alpha_{r;f}\beta_{r;\theta}}{2a\sqrt{\mu_0\rho}}, \frac{-\alpha_{r;f}\beta_{r;z}}{2a\sqrt{\mu_0\rho}}, \frac{\alpha_{r;f}}{2\rho a^2}\right]$$

$$L7_r = \left[0, 0, -\frac{\beta_{r;z}}{\sqrt{2}}, \frac{\beta_{r;\theta}}{\sqrt{2}}, 0, \frac{\beta_{r;z}}{\sqrt{2\mu_0\rho}}, -\frac{\beta_{r;\theta}}{\sqrt{2\mu_0\rho}}, 0\right]$$

$$L8_r = \left[0, \frac{\alpha_{r;f}C_{F;r}}{2a^2}, \frac{-\alpha_{r;s}C_{S;r}\beta_{r;\theta}\,\mathrm{Sgn}[B_r]}{2a^2}, \frac{-\alpha_{r;s}C_{S;r}\beta_{r;z}\,\mathrm{Sgn}[B_r]}{2a^2}, 0,\right.$$
$$\left.\frac{\alpha_{r;s}\beta_{r;\theta}}{2a\sqrt{\mu_0\rho}}, \frac{\alpha_{r;s}\beta_{r;z}}{2a\sqrt{\mu_0\rho}}, \frac{\alpha_{r;f}}{2\rho a^2}\right]$$

$$R1_r = \rho\left[\alpha_{r;f}, \frac{-\alpha_{r;f}C_{F;r}}{\rho}, \frac{\alpha_{r;s}C_{S;r}\beta_{r;\theta}\,\mathrm{Sgn}\,[B_r]}{\rho}, \frac{\alpha_{r;s}C_{S;r}\beta_{r;z}\,\mathrm{Sgn}[B_r]}{\rho}, 0,\right.$$
$$\left.\alpha_{r;s}a\beta_{r;\theta}\sqrt{\frac{\mu_0}{\rho}}, \alpha_{r;s}a\beta_{r;z}\sqrt{\frac{\mu_0}{\rho}}, a^2\alpha_{r;f}\right]$$

$$R2_r = \left[0, 0, \frac{-\beta_{r;z}}{\sqrt{2}}, \frac{\beta_{r;\theta}}{\sqrt{2}}, 0, \frac{-\beta_{r;z}\sqrt{\mu_0\rho}}{\sqrt{2}}, \frac{\beta_{r;\theta}\sqrt{\mu_0\rho}}{\sqrt{2}}, 0\right]$$

$$R3_r = \rho\left[\alpha_{r;s}, \frac{-\alpha_{r;s}C_{S;r}}{\rho}, \frac{-\alpha_{r;f}C_{F;r}\beta_{r;\theta}\,\mathrm{Sgn}[B_r]}{\rho}, \frac{-\alpha_{r;f}C_{F;r}\beta_{r;z}\,\mathrm{Sgn}[B_r]}{\rho}, 0,\right.$$
$$\left.-\alpha_{r;f}a\beta_{r;\theta}\sqrt{\frac{\mu_0}{\rho}}, -\alpha_{r;f}a\beta_{r;z}\sqrt{\frac{\mu_0}{\rho}}, a^2\alpha_{r;f}\right]$$

$$R4_r = [1, 0, 0, 0, 0, 0, 0, 0]$$

$$R5_r = [0, 0, 0, 0, 1, 0, 0, 0]$$

$$R6_r = \rho\left[\alpha_{r;s}, \frac{\alpha_{r;s}C_{\mathrm{S};r}}{\rho}, \frac{\alpha_{r;f}C_{\mathrm{F};r}\beta_{r;\theta}\,\mathrm{Sgn}[B_r]}{\rho}, \frac{\alpha_{r;f}C_{\mathrm{F};r}\beta_{r;z}\,\mathrm{Sgn}[B_r]}{\rho}, 0,\right.$$
$$\left. -\alpha_{r;f}a\beta_{r;\theta}\sqrt{\frac{\mu_0}{\rho}}, -\alpha_{r;f}a\beta_{r;z}\sqrt{\frac{\mu_0}{\rho}}, a^2\alpha_{r;f}\right]$$
$$R7_r = \left[0, 0, \frac{-\beta_{r;z}}{\sqrt{2}}, \frac{\beta_{r;\theta}}{\sqrt{2}}, 0, \frac{\beta_{r;z}\sqrt{\mu_0\rho}}{\sqrt{2}}, \frac{-\beta_{r;\theta}\sqrt{\mu_0\rho}}{\sqrt{2}}, 0\right]$$
$$R8_r = \rho\left[\alpha_{r;f}, \frac{\alpha_{r;f}C_{\mathrm{F};r}}{\rho}, \frac{-\alpha_{r;s}C_{\mathrm{S};r}\beta_{r;\theta}\,\mathrm{Sgn}[B_r]}{\rho}, \frac{-\alpha_{r;s}C_{\mathrm{S};r}\beta_{r;z}\,\mathrm{Sgn}[B_r]}{\rho}, 0,\right.$$
$$\left. \alpha_{r;s}a\beta_{r;\theta}\sqrt{\frac{\mu_0}{\rho}}, \alpha_{r;s}a\beta_{r;z}\sqrt{\frac{\mu_0}{\rho}}, a^2\alpha_{r;f}\right]$$

A.2. $\hat{z}$ direction

A.2.1. Eigenvalues (in non-decreasing order)

$$[w - C_{\mathrm{F};z}, w - C_{\mathrm{A};z}, w - C_{\mathrm{S};z}, w, w, w + C_{\mathrm{S};z}, w + C_{\mathrm{A};z}, w + C_{\mathrm{F};z}] \tag{A2}$$

A.2.2. Ortho-normalized eigenvectors

$$L1_z = \left[0, \frac{\alpha_{z;s}C_{\mathrm{S};z}\beta z; r\,\mathrm{Sgn}[B_z]}{2a^2}, \frac{\alpha_{z;s}C_{\mathrm{S};z}\beta_{z;\theta}\,\mathrm{Sgn}[B_z]}{2a^2}, \frac{-\alpha_{z;f}C_{\mathrm{F};z}}{2a^2}, \frac{\alpha_{z;s}\beta_{z;r}}{2a\sqrt{\mu_0\rho}}, \frac{\alpha_{z;s}\beta z;\theta}{2a\sqrt{\mu_0\rho}}, 0, \frac{\alpha_{z;f}}{2\rho a^2}\right]$$
$$L2_z = \left[0, \frac{-\beta_{z;\theta}}{\sqrt{2}}, \frac{\beta_{z;r}}{\sqrt{2}}, 0, \frac{-\beta_{z;\theta}}{\sqrt{2\mu_0\rho}}, \frac{\beta_{z;r}}{\sqrt{2\mu_0\rho}}, 0, 0\right]$$
$$L3_z = \left[0, \frac{-\alpha_{z;f}C_{\mathrm{F};z}\beta z; r\,\mathrm{Sgn}[B_z]}{2a^2}, \frac{-\alpha_{z;f}C_{\mathrm{F};z}\beta_{z;\theta}\,\mathrm{Sgn}[B_z]}{2a^2}, \frac{-\alpha_{z;s}C_{\mathrm{S};z}}{2a^2},\right.$$
$$\left. \frac{-\alpha_{z;f}\beta_{z;r}}{2a\sqrt{\mu_0\rho}}, \frac{-\alpha_{z;f}\beta z;\theta}{2a\sqrt{\mu_0\rho}}, 0, \frac{\alpha_{z;s}}{2\rho a^2}\right]$$
$$L4_z = [0, 0, 0, 0, 0, 0, 1, 0]$$
$$L5_z = [1, 0, 0, 0, 0, 0, 0, \frac{-1}{a^2}]$$
$$L6_z = \left[0, \frac{\alpha_{z;f}C_{\mathrm{F};z}\beta z; r\,\mathrm{Sgn}[B_z]}{2a^2}, \frac{\alpha_{z;f}C_{\mathrm{F};z}\beta_{z;\theta}\,\mathrm{Sgn}[B_z]}{2a^2}, \frac{\alpha_{z;s}C_{\mathrm{S};z}}{2a^2}, \frac{-\alpha_{z;f}\beta_{z;r}}{2a\sqrt{\mu_0\rho}}, \frac{-\alpha_{z;f}\beta z;\theta}{2a\sqrt{\mu_0\rho}}, 0, \frac{\alpha_{z;s}}{2\rho a^2}\right]$$
$$L7_z = \left[0, \frac{-\beta_{z;\theta}}{\sqrt{2}}, \frac{\beta_{z;r}}{\sqrt{2}}, 0, \frac{\beta_{z;\theta}}{\sqrt{2\mu_0\rho}}, \frac{-\beta_{z;r}}{\sqrt{2\mu_0\rho}}, 0, 0\right]$$
$$L8_z = \left[0, \frac{-\alpha_{z;s}C_{\mathrm{S};z}\beta z; r\,\mathrm{Sgn}[B_z]}{2a^2}, \frac{-\alpha_{z;s}C_{\mathrm{S};z}\beta_{z;\theta}\,\mathrm{Sgn}[B_z]}{2a^2}, \frac{\alpha_{z;f}C_{\mathrm{F};z}}{2a^2}, \frac{\alpha_{z;s}\beta_{z;r}}{2a\sqrt{\mu_0\rho}}, \frac{\alpha_{z;s}\beta z;\theta}{2a\sqrt{\mu_0\rho}}, 0, \frac{\alpha_{z;f}}{2\rho a^2}\right]$$

$$R1_z = \rho \left[\alpha_{z;f}, \frac{\alpha_{z;s} C_{S;z} \beta_{z;r} \operatorname{Sgn}[B_z]}{\rho}, \frac{\alpha_{z;s} C_{S;z} \beta_{z;\theta} \operatorname{Sgn}[B_z]}{\rho}, \frac{-\alpha_{z;f} C_{F;z}}{\rho}, \right.$$
$$\left. \alpha_{z;s} a \beta_{z;r} \sqrt{\frac{\mu_0}{\rho}}, \alpha_{z;s} a \beta_{z;\theta} \sqrt{\frac{\mu_0}{\rho}}, 0, a^2 \alpha_{z;f} \right]$$

$$R2_z = \left[0, \frac{-\beta_{z;\theta}}{\sqrt{2}}, \frac{\beta_{z;r}}{\sqrt{2}}, 0, \frac{-\beta_{z;\theta}\sqrt{\mu_0 \rho}}{\sqrt{2}}, \frac{\beta_{z;r}\sqrt{\mu_0 \rho}}{\sqrt{2}}, 0, 0 \right]$$

$$R3_z = \rho \left[\alpha_{z;s}, \frac{-\alpha_{z;f} C_{F;z} \beta_{z;r} \operatorname{Sgn}[B_z]}{\rho}, \frac{-\alpha_{z;f} C_{F;z} \beta_{z;\theta} \operatorname{Sgn}[B_z]}{\rho}, \frac{-\alpha_{z;s} C_{S;z}}{\rho}, \right.$$
$$\left. -\alpha_{z;f} a \beta_{z;r} \sqrt{\frac{\mu_0}{\rho}}, -\alpha_{z;f} a \beta_{z;\theta} \sqrt{\frac{\mu_0}{\rho}}, 0, a^2 \alpha_{z;s} \right]$$

$$R4_z = [0, 0, 0, 0, 0, 0, 1, 0]$$

$$R5_z = [1, 0, 0, 0, 0, 0, 0, 0]$$

$$R6_z = \rho \left[\alpha_{z;s}, \frac{\alpha_{z;f} C_{F;z} \beta_{z;r} \operatorname{Sgn}[B_z]}{\rho}, \frac{\alpha_{z;f} C_{F;z} \beta_{z;\theta} \operatorname{Sgn}[B_z]}{\rho}, \frac{\alpha_{z;s} C_{S;z}}{\rho}, \right.$$
$$\left. -\alpha_{z;f} a \beta_{z;r} \sqrt{\frac{\mu_0}{\rho}}, -\alpha_{z;f} a \beta_{z;\theta} \sqrt{\frac{\mu_0}{\rho}}, 0, a^2 \alpha_{z;s} \right]$$

$$R7_z = \left[0, \frac{-\beta_{z;\theta}}{\sqrt{2}}, \frac{\beta_{z;r}}{\sqrt{2}}, 0, \frac{\beta_{z;\theta}\sqrt{\mu_0 \rho}}{\sqrt{2}}, \frac{-\beta_{z;r}\sqrt{\mu_0 \rho}}{\sqrt{2}}, 0, 0 \right]$$

$$R8_z = \rho \left[\alpha_{z;f}, \frac{-\alpha_{z;s} C_{S;z} \beta_{z;r} \operatorname{Sgn}[B_z]}{\rho}, \frac{-\alpha_{z;s} C_{S;z} \beta_{z;\theta} \operatorname{Sgn}[B_z]}{\rho}, \frac{\alpha_{z;f} C_{F;z}}{\rho}, \right.$$
$$\left. \alpha_{z;s} a \beta_{z;r} \sqrt{\frac{\mu_0}{\rho}}, \alpha_{z;s} a \beta_{z;\theta} \sqrt{\frac{\mu_0}{\rho}}, 0, a^2 \alpha_{z;f} \right]$$

REFERENCES

1. Jahn RG. *Physics of Electric Propulsion*. McGraw-Hill: New York, 1968.
2. Polk JE. Mechanisms of cathode erosion in plasma thrusters. *PhD Thesis*, Princeton University, 1995.
3. Sutton GP. *Rocket Propulsion Elements*. Wiley: New York, 1992.
4. Jahn RG, Choueiri EY. Electric propulsion, in *Encyclopedia of Physical Science and Technology*, 3rd Edition, Academic press, San Diego, vol. 5, pp. 125–141, 2002.
5. Choueiri EY. Scaling of thrust in self-field magnetoplasmadynamic thrusters. *Journal of Propulsion and Power* 1998; **14**(5):744–753.
6. Martinache HC. A theory on the parallel-plate plasma accelerator. *PhD Thesis*, Princeton University, 1974.
7. Villani DD. Energy loss mechanisms in a magnetoplasmadynamic arcjet. *PhD Thesis*, Princeton University, 1982.
8. Sankaran K. Simulation of MPD flows using a flux-limited numerical method for the MHD equations. *Master's Thesis*, Mechanical and Aerospace Engineering Department, Princeton University, 2001.
9. Toki K, Kimura I, Tanaka M. Current distribution on the electrodes on MPD arcjets. *AIAA Journal* 1982; **20**(7):889.
10. Ao T, Fujiwara T. Numerical and experimental study of an MPD thruster. *IEPC*-84-08, 1984.

11. Miyasaka T, Fujiwara T. Numerical prediction of onset phenomenon in a 2-dimensional axisymmetric MPD thruster. *AIAA*-99-2432, 1999.
12. Caldo G. Numerical simulation of MPD thruster flows with anomalous transport. *Master's Thesis*, Princeton University, 1994.
13. Choueiri EY. Anomalous resistivity and heating in current-driven plasma thrusters. *Physics of Plasmas* 1999; **6**(5):2290.
14. LaPointe M. Numerical simulation of geometric scale effects in cylindrical self-field MPD thrusters. *NASA-CR*-189224, 1992.
15. Chanty JMG, Martinez-Sanchez M. Two-dimensional numerical simulation of MPD flows. *AIAA*-87-1090, 1987.
16. Niewood EH. An explanation for anode voltage drops in an MPD thruster. *PhD Thesis*, MIT, 1993.
17. Turchi PJ, Mikellides PG, Hohman KW, Leiweke RJ, Mikellides IG, Schmahl CS, Roderick NF, Peterkin Jr RE. Progress in modeling plasma thrusters and related flows. *IEPC*-95-159, 1995.
18. Lilekis DC, Peterkin Jr RE. Effects of azimuthal injection asymmetry of MPD thruster performance using MACH3 code. *IEPC*-95-2677, 1995.
19. Auweter-Kurtz M, Kurtz HL, Schrade HO, Sleziona PC. Numerical modeling of the flow discharge in MPD thrusters. *Journal of Propulsion and Power* 1989; **51**:49–55.
20. Boie C, Kaeppeler HJ, Auweter-Kurtz M, Sleziona PC. Application of adaptive numerical schemes for MPD thruster simulation. *IEPC*-97-115, 1997.
21. Heiermann J, Auweter-Kurtz M, Kaeppeler HJ, Eberle A, Iben U, Sleziona PC. Recent improvements in numerical methods for the simulation of MPD thruster flows on adaptive meshes. *IEPC*-99-169, 1999.
22. Myong RS. Theoretical and computational investigation of nonlinear waves in magnetohydrodynamics. *PhD Thesis*, University of Michigan, 1996.
23. Shumlak U, Jones O, Eberhardt SD. An implicit scheme for nonideal magnetohydrodynamics. *Journal of Computational Physics* 1997; **130**:231–242.
24. Brackbill JU, Barnes DC. The effect of non-zero $\nabla \cdot \mathbf{B}$ on the numerical solution of the magnetohydrodynamic equations. *Journal of Computational Physics* 1980; **35**:426.
25. Powell KG. An approximate Riemann solver for magnetohydrodynamics (that works in more than one dimension). *NASA ICASE Report* 94–24, 1994.
26. Powell KG. An Upwind Scheme for Magnetohydrodynamics. *AIAA*-95-1704, 1995.
27. Powell KG. A solution-adaptive upwind scheme for ideal magnetohydrodynamics. *Journal of Computational Physics* 1999; **154**:284–309.
28. van Leer B, Tai CH, Powell KG. Design of optimally smoothing multi-stage schemes for the Euler equations. *AIAA*-89-1933, 1999.
29. Martinelli L. Calculations of viscous flows with a multigrid method. *PhD Thesis*, Princeton University, 1987.
30. Godunov SK. Finite difference method for numerical computation of discontinuous solution of the equation of fluid dynamics. *Matematicheskii Sbornik* 1959; **47**:15–21.
31. Godunov SK. Symmetric form of the equations of magnetohydrodynamics. In *Numerical Methods for Mechanics of Continuum Medium*, Report of the Computer Center of the Siberian Branch of the USSR Academy of Sciences, 1972.
32. Boris JP, Book DL. Solutions of continuity equations by the method of flux corrected transport. *Journal of Computational Physics* 1976; **16**:85.
33. Roe P. Approximate Riemann solvers, parameter vectors, and difference schemes. *Journal of Computational Physics* 1981; **43**:357.
34. Roe P. Characteristics-based schemes for the Euler equations. *Annual Review of Fluid Mechanics* 1986; **18**:337.
35. Laney CB. *Computational Gasdynamics*. Cambridge University Press: Cambridge, 1998.
36. Jameson A. Analysis and design of numerical schemes for gas dynamics, 1: artificial diffusion, upwind biasing, limiters and their effect on accuracy and multigrid convergence. *Computational Fluid Dynamics* 1995; **4**:171–218.
37. Cargo P, Gallice G. Roe matrices for ideal MHD and systematic construction of Roe matrices for systems of conservation laws. *Journal of Computational Physics* 1997; **136**:446.
38. Aslan N. Two-dimensional solutions of MHD equations with an adapted Roe method. *International Journal for Numerical Methods in Fluids* 1996; **23**(11):1211.
39. Sod GA. A survey of finite-difference methods for systems of nonlinear conservation laws. *Journal of Computational Physics* 1978; **27**:1.
40. Brio M, Wu CC. An upwind differencing scheme fot the equations of ideal MHD. *Journal of Computational Physics* 1988; **75**.
41. Taylor JB. Relaxation of toroidal plasma and generation of reverse magnetic fields. *Physical Review Letters* 1974; **33**(19):1139–1141.

